Vol 455|16 October 2008|doi:10.1038/nature07311

LETTERS

The type IV mucolipidosis-associated protein TRPML1 is an endolysosomal iron release channel

Xian-Ping Dong[1], Xiping Cheng[1], Eric Mills[1], Markus Delling[2], Fudi Wang[3], Tino Kurz[4] & Haoxing Xu[1]

TRPML1 (mucolipin 1, also known as MCOLN1) is predicted to be an intracellular late endosomal and lysosomal ion channel protein that belongs to the mucolipin subfamily of transient receptor potential (TRP) proteins[1–3]. Mutations in the human *TRPML1* gene cause mucolipidosis type IV disease (ML4)[4,5]. ML4 patients have motor impairment, mental retardation, retinal degeneration and iron-deficiency anaemia. Because aberrant iron metabolism may cause neural and retinal degeneration[6,7], it may be a primary cause of ML4 phenotypes. In most mammalian cells, release of iron from endosomes and lysosomes after iron uptake by endocytosis of Fe^{3+}-bound transferrin receptors[6], or after lysosomal degradation of ferritin–iron complexes and autophagic ingestion of iron-containing macromolecules[6,8], is the chief source of cellular iron. The divalent metal transporter protein DMT1 (also known as SLC11A2) is the only endosomal Fe^{2+} transporter known at present and it is highly expressed in erythroid precursors[6,9]. Genetic studies, however, suggest the existence of a DMT1-independent endosomal and lysosomal Fe^{2+} transport protein[9]. By measuring radiolabelled iron uptake, by monitoring the levels of cytosolic and intralysosomal iron and by directly patch-clamping the late endosomal and lysosomal membrane, here we show that TRPML1 functions as a Fe^{2+} permeable channel in late endosomes and lysosomes. ML4 mutations are shown to impair the ability of TRPML1 to permeate Fe^{2+} at varying degrees, which correlate well with the disease severity. A comparison of *TRPML1*$^{-/-}$ ML4 and control human skin fibroblasts showed a reduction in cytosolic Fe^{2+} levels, an increase in intralysosomal Fe^{2+} levels and an accumulation of lipofuscin-like molecules in *TRPML1*$^{-/-}$ cells. We propose that TRPML1 mediates a mechanism by which Fe^{2+} is released from late endosomes and lysosomes. Our results indicate that impaired iron transport may contribute to both haematological and degenerative symptoms of ML4 patients.

Release of Fe^{2+} from late endosomes and lysosomes into the cytosol is essential for cellular iron metabolism (see Supplementary Fig. 1)[6]. Because TRPML1 is ubiquitously expressed (in cells of every tissue)[5] and primarily localized in the late endosome and lysosome (LEL)[1,3,10], we propose that TRPML1 may act as an endolysosomal Fe^{2+} release channel. The intracellular localization of wild-type TRPML1 (refs 1, 3 and 10; see also Supplementary Fig. 2), however, makes it difficult to assay the function of this channel. To overcome this problem, we recently developed a functional assay for TRPML channels[11]. A spontaneous mouse mutation (A419P)[12] markedly increases TRPML3-mediated currents at the plasma membrane without altering its permeation properties[11]. Mice carrying this mutation (varitint-waddler, *Va*) are deaf and show skin pigmentation defects. When the *Va* mutation (proline substitution) was introduced into a homologous position in TRPML1 (V432P), the mutant channel TRPML1^{Va} was (mis)localized in many cellular compartments including both LEL and the plasma membrane (Supplementary Fig. 2). Notably, TRPML1^{Va}, but not wild-type TRPML1, generated a cationic whole-cell current that can be measured by patch clamp[11].

We studied TRPML proteins by transiently expressing them in HEK293T cell lines. To monitor expression, TRPML channels were fused to enhanced green fluorescent protein (EGFP) at their amino termini. In response to a voltage step protocol, TRPML1^{Va}-expressing cells showed strong inwardly rectifying step currents (Fig. 1a and Supplementary Fig. 3) in a standard extracellular bath solution (a modified Tyrode's solution). TRPML1^{Va}-mediated current ($I_{TRPML1^{Va}}$) was 101 ± 8.6 pA pF^{-1} at -80 mV (mean $\pm$ s.e.m., $n = 48$). To mimic the acidic environments of lysosomes where the extracellular side (analogous to the intralysosomal luminal side) of the wild-type TRPML1 protein is exposed to, extracellular solutions were adjusted to pH 4.6. No sizable inward current was detected when *N*-methyl-D-glucamine ($NMDG^+$) was the only major cation in the bath (pH 4.6; Fig. 1b), indicating that $I_{TRPML1^{Va}}$ is a proton-impermeable cationic current[11]. Bath perfusion of 30 mM extracellular $[Fe^{2+}]$ ($[Fe^{2+}]_o$, pH 4.6) to TRPML1^{Va}-expressing cells induced large inwardly rectifying currents (Fig. 1c). The current density of $[Fe^{2+}]_o$-elicited $I_{TRPML1^{Va}}$ ($I_{Fe/TRPML1^{Va}}$) at -80 mV was 74 ± 8.6 pA pF^{-1} (mean $\pm$ s.e.m., $n = 24$). To keep Fe^{2+} in a reduced state, ascorbic acid was used as the counter anion in the bath solution. The only other main cation in the 30 mM Fe^{2+} solution was $NMDG^+$. Thus, $I_{Fe/TRPML1^{Va}}$ is carried solely by Fe^{2+}. Consistent with this, the amplitude of $I_{Fe/TRPML1^{Va}}$ was strongly dependent on $[Fe^{2+}]_o$ (Supplementary Fig. 4).

Both $I_{Fe/TRPML1^{Va}}$ (Fig. 1e) and $I_{TRPML1^{Va}}$[11] were enhanced at low pH. Compared to experiments conducted at physiological pH (7.4), $I_{Fe/TRPML1^{Va}}$ was enhanced ~2-fold at pH 4.6 (approximately the luminal pH of lysosomes). In cells transfected with TRPML2^{Va} (a short splice variant; see Methods), a large current (23.0 ± 3.8 pA pF^{-1} at -80 mV, $n = 7$) was evoked by 30 mM Fe^{2+} (pH 4.6, Fig. 1e). Similar to $I_{TRPML1^{Va}}$, $I_{TRPML2^{Va}}$ was also strongly potentiated by low pH (Supplementary Fig. 5). The ratio of I_{Fe}/I_{Tyrode} for TRPML2^{Va} was $139 \pm 22\%$ (at -80 mV, $n = 7$), which was even larger than the ratio for TRPML1^{Va} ($72 \pm 7\%$, $n = 11$). In contrast with TRPML1^{Va} and TRPML2^{Va}, the ratio of I_{Fe}/I_{Tyrode} for TRPML3^{Va} was only $2.3 \pm 0.2\%$ ($n = 8$; Fig. 1f). Thus, Fe^{2+} permeability is specific for TRPML1 and TRPML2, but not for the closely related TRPML3. Cationic selectivity analysis suggested that TRPML1^{Va} was also permeable to most other divalent trace metals including Mn^{2+} and Zn^{2+}, but not to Fe^{3+} (Supplementary Fig. 6). Detailed analyses of the permeation properties of TRPML1^{Va} suggested that the conduction mechanism of Fe^{2+} resembled those of Na^+ and Ca^{2+} (see Supplementary Figs 7–9).

[1]The Department of Molecular, Cellular, and Developmental Biology, The University of Michigan, 3089 Natural Science Building (Kraus), 830 North University, Ann Arbor, Michigan 48109, USA. [2]The Department of Cardiology, Children's Hospital Boston, Enders 1350, 320 Longwood Avenue, Boston, Massachusetts 02115, USA. [3]Institute for Nutritional Sciences, Shanghai Institutes for Biological Sciences, Chinese Academy of Sciences, Shanghai 200031, China. [4]Department of Pharmacology, Faculty of Health Science, University of Linköping, S-58185 Linköping, Sweden.

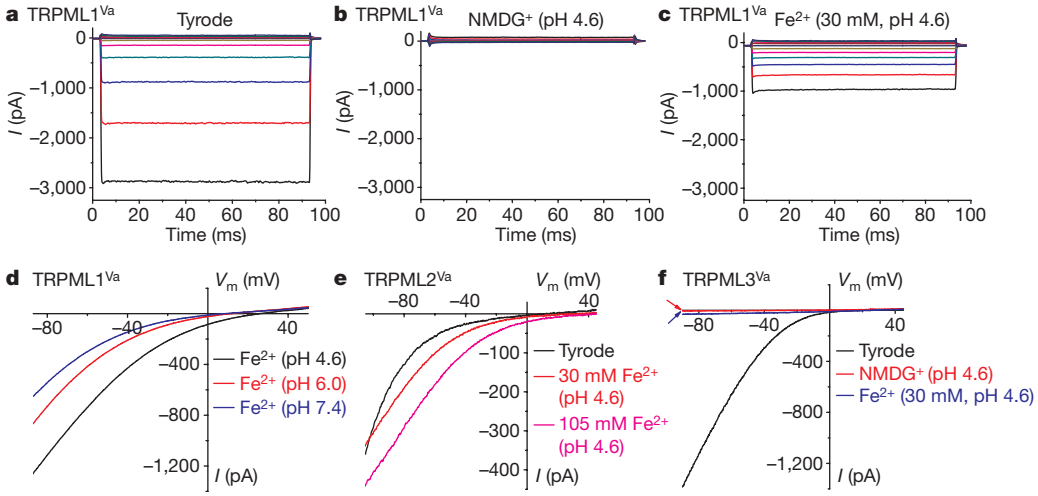

Figure 1 | TRPML1^{Va}-expressing cells have a constitutively active H$^+$-modulated Fe^{2+} current. **a**, A TRPML1^{Va}-expressing HEK293T cell showed a large inwardly rectifying whole-cell current elicited by voltage steps (from −140 mV to +80 mV in increments of 20 mV) in the standard extracellular (Tyrode's) bath solution. Step duration, 90 ms; holding potential, 0 mV; V_m, membrane potential. **b**, No significant inward current was detected in NMDG$^+$ (Na^+-free, Ca^{2+}-free, pH 4.6) solution. **c**, Inwardly rectifying step currents were evoked by 30 mM Fe^{2+} solution (pH 4.6) in the same cell as shown in **a** and **b**. **d**, pH-dependence of $I_{Fe/TRPML1^{Va}}$. Whole-cell currents were elicited by repeated voltage ramps (−100 to +100 mV; 400 ms) with a 4-s interval between ramps. Only a portion of the voltage protocol is shown. Holding potential, 0 mV. **e**, Large $I_{Fe/TRPML2^{Va}}$ was seen in the presence of 30 and 105 mM Fe^{2+} (pH 4.6). **f**, Little or no I_{Fe} was seen in a TRPML3^{Va}-expressing cell.

Next, we tested whether the Fe^{2+} permeability of TRPML1 is impaired by ML4 mutations. More than 15 ML4 mutations have been identified, most of which are located in the transmembrane regions of TRPML1 (Supplementary Fig. 10)[4,5,13,14]. We constructed six of these ML4 mutants into the TRPML1^{Va} background and investigated the Fe^{2+} permeability of these combined mutations. We found that all ML4 mutant TRPML1^{Va} channels had significantly smaller I_{Fe} than TRPML1^{Va}. In particular, T232P, D362Y and V446L mutations (combined with the *Va* mutation) completely eliminated I_{Fe}, as well as I_{Tyrode} (Fig. 2a and Supplementary Fig. 11), although the protein expression levels and subcellular localization pattern of these mutants were similar to those of the parental TRPML1^{Va} protein (Supplementary Figs 12 and 13). Patients carrying these mutations are reported to have severe phenotypes[5,15]. On the other hand, a large I_{Fe} was detected in F408Δ-TRPML1^{Va}-transfected cells. The average current density of this mutant, however, was still significantly smaller than $I_{Fe/TRPML1^{Va}}$. Patients carrying the F408Δ mutation have unusually mild phenotypes[13,15]. Small but evident I_{Fe} was detected with expression of two other mutants (R403C and F465L). A patient carrying the R403C mutation was reported to have a relatively mild phenotype[14]. Taken together, these results

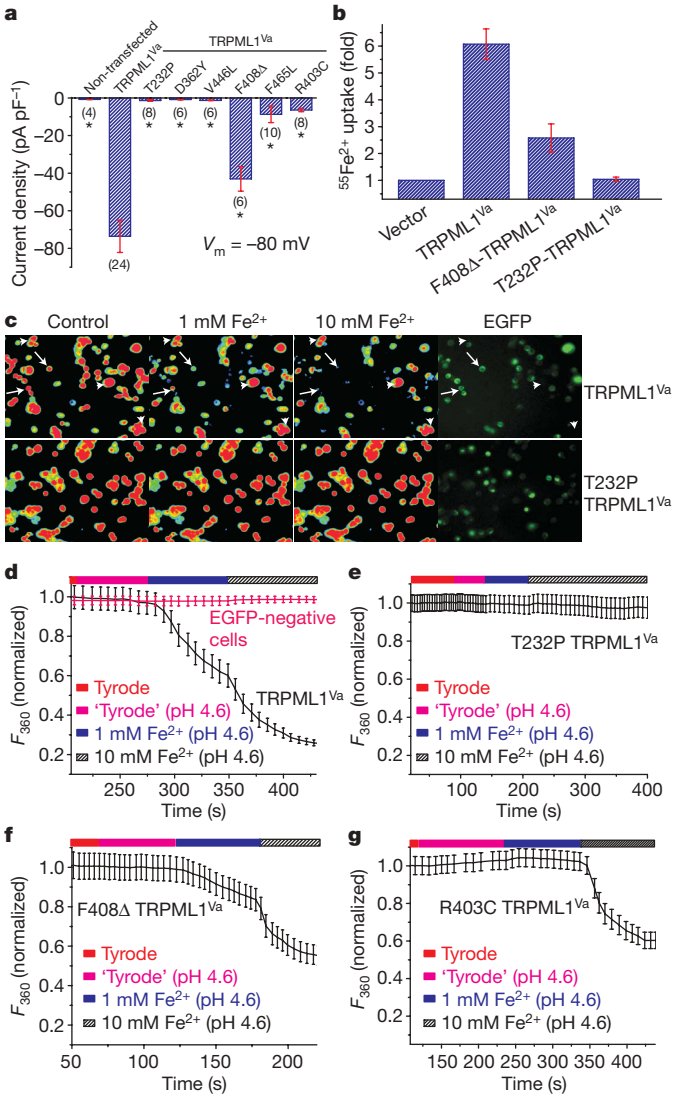

Figure 2 | Fe^{2+} permeability of the TRPML1 channel is impaired by ML4 mutations. **a**, Current densities (mean ± s.e.m., n = 4–10) of I_{Fe} (30 mM Fe^{2+}, pH 4.6) for TRPML1^{Va} and ML4 mutant TRPML1^{Va} channels. Asterisk indicates statistical difference ($P < 0.01$) compared to TRPML1^{Va}. **b**, $^{55}Fe^{2+}$ uptake (normalized) in HEK293T cells transfected with vector control, with TRPML1^{Va}, with F408Δ-TRPML1^{Va} and with T232P-TRPML1^{Va} constructs. Error bars indicate the standard deviation on the basis of two independent triplicate experiments. **c**, $[Fe^{2+}]_o$-dependent quenching of Fura-2 fluorescence in TRPML1^{Va}-transfected cells (arrows), but not in non-transfected control cells (arrowheads) or T232P-TRPML1^{Va}-transfected cells (bottom row). The fluorescence intensity was measured at an excitation wavelength of 360 nm (F_{360}). The original magnification used for all micrographs was ×200. **d**, Average normalized responses of EGFP-positive TRPML1^{Va}-transfected cells (typically n = 20–40 cells) to 1 or 10 mM Fe^{2+} (pH 4.6). **e**, No significant quenching was seen in T232P-TRPML1^{Va}-transfected cells. **f**, Slightly less quenching was observed for the F408Δ-TRPML1^{Va}-expressing cells. **g**, A small but significant quenching reaction was detected (with 10 mM Fe^{2+}) in R403C-TRPML1^{Va}-expressing cells.

indicate that ML4 mutations significantly impair the Fe^{2+} permeability of TRPML1. The degree of the impaired Fe^{2+} permeability seems to correlate well with disease severity observed in ML4 patients.

To investigate $TRPML1^{Va}$-mediated Fe^{2+} influx under less invasive conditions in intact cells, we measured $^{55}Fe^{2+}$ uptake at low pH (pH 5.8, 1 μM $^{55}Fe^{2+}$; Fig. 2b). Significant $^{55}Fe^{2+}$ uptake was seen in HEK293T cells transfected with $TRPML1^{Va}$, but not with T232P-$TRPML1^{Va}$. An intermediate $^{55}Fe^{2+}$ uptake was seen for F408Δ-$TRPML1^{Va}$. These results indicate that $TRPML1^{Va}$ can mediate significant Fe^{2+} entry even at micromolar $[Fe^{2+}]_o$. We also adopted a fluorescence-based Fe^{2+} quenching assay to measure $TRPML1^{Va}$-mediated Fe^{2+} entry in HEK293T cells. Heavy metals such as Mn^{2+} and Fe^{2+} can bind Ca^{2+}-sensitive dyes such as Fura-2 with higher affinity, resulting in strong fluorescence quenching effects[16]. Substantial quenching of Fura-2 fluorescence was seen in $TRPML1^{Va}$-expressing cells after the addition of 1 mM Fe^{2+} (pH 4.6; Fig. 2d, f). Increased quenching was observed with the addition of higher concentrations of Fe^{2+} (10 mM, pH 4.6). In contrast, no significant quenching was detected in neighbouring non-transfected EGFP-negative cells or $TRPML3^{Va}$-transfected cells (1 mM Fe^{2+}; Supplementary Fig. 14). ML4 mutant $TRPML1^{Va}$-expressing HEK293T cells showed an impairment of Fe^{2+} quenching. No significant Fe^{2+} quenching was seen in T232P- (Fig. 2e), D362Y-, or V446L-$TRPML1^{Va}$-expressing cells (data not shown). Slightly less quenching was observed for F408Δ-$TRPML1^{Va}$ (Fig. 2f). In contrast, R403C-$TRPML1^{Va}$ (Fig. 2g) and F465L-$TRPML1^{Va}$ showed no response to the addition of 1 mM Fe^{2+}. However, a higher concentration of Fe^{2+} (10 mM) induced a slow but significant quenching. These results agree with the electrophysiological measurements of ML4 mutants, as well as the disease severity of ML4 patients carrying

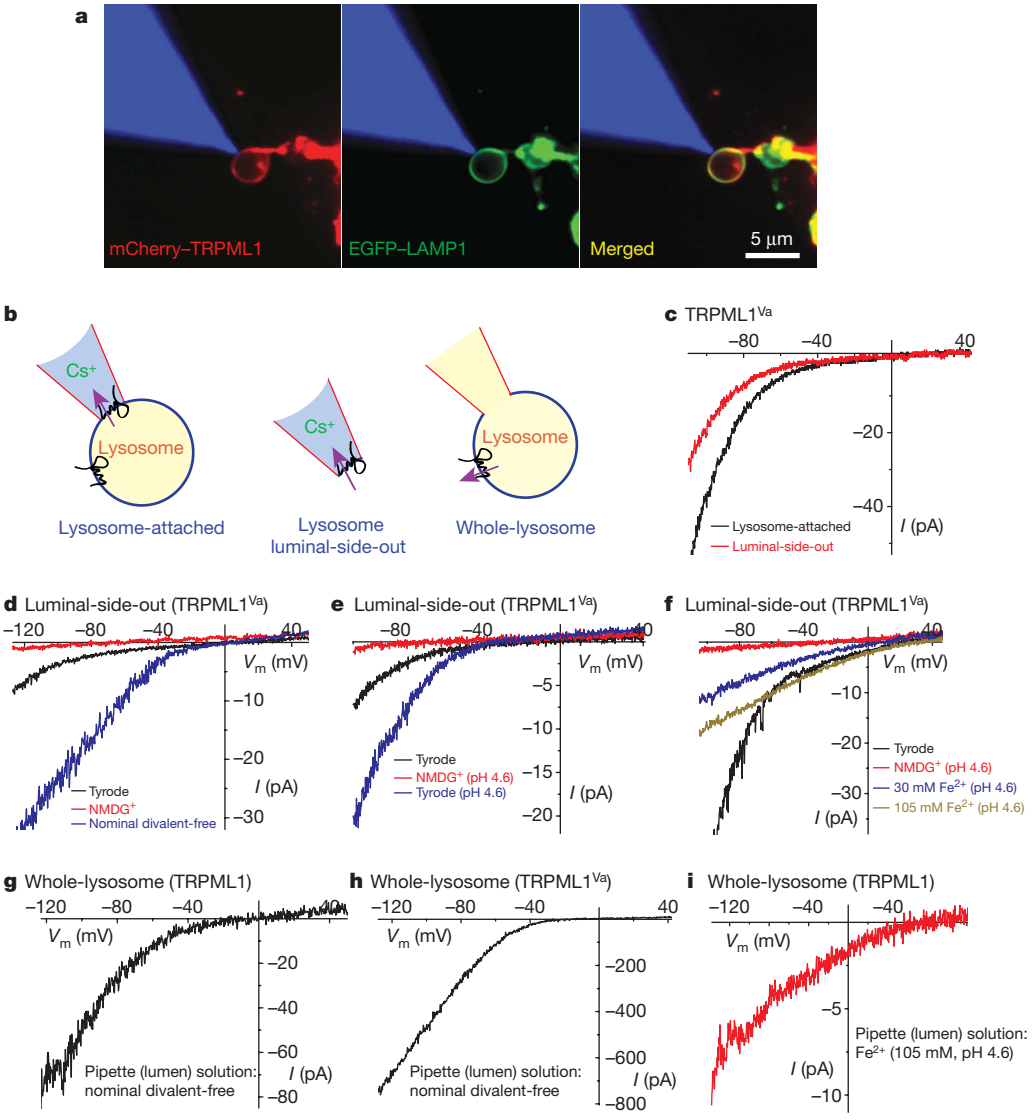

Figure 3 | TRPML1 conducts Fe^{2+} in late endosomes and lysosomes. **a**, Co-localization of mCherry–TRPML1 and EGFP–LAMP1 at the membrane of an isolated enlarged LEL (see Methods). The patch pipette was filled with red rhodamine B dye (shown in blue for the purpose of illustration). **b**, Cartoons of three distinct patch-clamp configurations of lysosomal recordings: lysosome-attached, lysosome luminal-side-out and whole-lysosome. In each configuration, the pink arrow indicates the direction of the inward (at negative potentials; flow out of the lysosomes) current mediated by TRPML1 (as shown in **c**–**i**). **c**, Lysosomal $I_{TRPML1^{Va}}$. Switching from lysosome-attached to (lysosome) luminal-side-out configuration significantly reduced the amplitude of the current. The luminal-side-out patch was exposed to the Tyrode's solution. A Cs^+-based solution (147 mM Cs-methanesulphonate (Cs-MSA)) was used as a pipette solution for both configurations. **d**, $NMDG^+$-impermeable lysosomal $I_{TRPML1^{Va}}$ was much larger in the absence of divalent cations (nominal divalent-free). **e**, Lowering pH potentiated lysosomal $I_{TRPML1^{Va}}$. **f**, $I_{Fe/TRPML1^{Va}}$ induced by 30 mM and 105 mM Fe^{2+}. **g**, Whole-lysosome current in an enlarged lysosome expressing wild-type TRPML1. The pipette (lumen) solution contained nominal divalent-free Tyrode solution. A Cs^+-based bath solution (147 mM Cs-MSA) was used. **h**, Whole-lysosome $I_{TRPML1^{Va}}$. **i**, Whole-lysosome $I_{Fe/TRPML1}$. The pipette (lumen) solution contained 105 mM Fe^{2+} (pH 4.6).

these mutations[5,13–15]. Thus, ML4 phenotypes result from a loss-of-function of TRPML1 with respect to Fe^{2+} and/or Ca^{2+} permeability.

To validate our use of $TRPML1^{Va}$ as a model to extrapolate potential intracellular functions of wild-type TRPML1, and more importantly, to confirm whether wild-type TRPML1 conducts Fe^{2+} from the lumen of LEL into the cytosol, we performed patch-clamp recordings directly on native LEL membranes (Fig. 3a and Supplementary Fig. 15; see Methods). In $TRPML1^{Va}$-positive enlarged LEL, large inwardly rectifying currents were seen under the lysosome-attached configuration (Fig. 3b, c). The currents became smaller when the patch was excised (lysosome luminal-side-out) and exposed to Tyrode's solution (Fig. 3c). These large inwardly rectifying currents were not seen in $TRPML1^{Va}$-negative vacuoles, suggesting that these lysosomal currents are mediated by $TRPML1^{Va}$ (hereafter referred to as lysosomal $I_{TRPML1^{Va}}$). Note that inward lysosomal currents are actually currents that flow out of the lysosomes. Similar to $I_{TRPML1^{Va}}$ recorded at the plasma membrane, lysosomal $I_{TRPML1^{Va}}$ was impermeable to $NMDG^+$ and H^+, but was potentiated by low pH or by removal of divalent cations in the bath solution (nominal divalent-free; Fig. 3d, e). When the luminal-side-out patches were exposed to 30 mM or 105 mM Fe^{2+} solutions (pH 4.6), smaller and less rectifying currents were seen, resembling $I_{Fe/TRPML1^{Va}}$ at the plasma membrane. These results indicate that $TRPML1^{Va}$ behaves similarly at both plasma and lysosomal membranes. Likewise, ML4 mutant $TRPML1^{Va}$ channels also behaved similarly as their plasma membrane counterparts (Supplementary Fig. 16), consistent with our conclusion that ML4 mutations primarily affect the channel function of TRPML1.

Next we performed whole-lysosome recordings on enlarged LEL expressing wild-type TRPML1 and $TRPML1^{Va}$. Significant inwardly rectifying currents were seen in wild-type TRPML1-positive LEL (81.0 ± 9.0 pA pF^{-1} at -120 mV, $n = 6$; Fig. 3g) with nominal divalent-free solution in the luminal side (that is, pipette solution), although the current amplitude is still one order of magnitude smaller than the whole-lysosome current recorded from $TRPML1^{Va}$-positive LEL ($1{,}713 \pm 404$ pA pF^{-1} at -120 mV, $n = 4$; Fig. 3h). Because we were not able to record any significant whole-cell current from wild-type TRPML1-expressing HEK293T cells[11], our results indicate that the *Va* mutation affects both channel gating and trafficking (between LEL and the plasma membrane) of TRPML1. When isotonic (105 mM) Fe^{2+} solution was included in the luminal side of wild-type TRPML1-positive enlarged LEL, inwardly rectifying currents with very positive reversal potential were observed (18 ± 4 pA pF^{-1} at -120 mV, $n = 4$; Fig. 3i). Collectively, these results indicate that wild-type TRPML1 is a lysosomal Fe^{2+}-permeable channel, and that the *Va* mutation does not alter the permeation properties of the TRPML1 channel.

Retention of Fe^{2+} in LEL due to loss or inactivation of the Fe^{2+} release mechanism may result in an insufficient supply of cytosolic Fe^{2+}. We therefore measured the levels of free (chelatable) intracellular Fe^{2+} in skin fibroblasts from a ML4 patient ($TRPML1^{-/-}$) and the non-diseased parent ($TRPML1^{+/-}$) using a fluorescence-based iron de-quenching imaging method (see Methods)[17]. Chelatable Fe^{2+} levels were significantly lower in $TRPML1^{-/-}$ cells compared to the control $TRPML1^{+/-}$ cells (Fig. 4a, b). TRPML1-deficient skin fibroblast cells show autofluorescence (Fig. 4c) at excitation wavelengths between 440 nm and 500 nm, reminiscent of accumulated lipofuscin-like substances previously reported[18]. The autofluorescence observed was primarily localized in LAMP1 (a marker for LEL)-positive compartments (Fig. 4c), indicative of a lysosomal dysfunction in $TRPML1^{-/-}$ cells. Lipofuscin, also referred to as an 'ageing pigment', is a non-degradable oxidized polymeric substance containing proteins, lipids, carbohydrates and iron[19]. The production of lipofuscin is facilitated by increased intralysosomal Fe^{2+} levels[19]. Our results indicate that an accumulation of autofluorescent lipofuscin-like molecules in $TRPML1^{-/-}$ cells might result from impaired intralysosomal iron metabolism. Consistent with this, lysosomal iron staining experiments showed that $TRPML1^{-/-}$ cells had higher lysosomal iron content than control cells (Supplementary Fig. 17).

We have demonstrated that TRPML1 has a critical role in cellular iron homeostasis by showing the cytosolic Fe^{2+} deficiency with concurrent intralysosomal iron overload in ML4 cells. ML4 cells show a defect in the late endocytic pathway[10,20,21], suggesting that TRPML1 may be required for Ca^{2+}-dependent fusion or fission of LEL. However, this defect in vesicular transport cannot explain the cytosolic Fe^{2+} deficiency that we observed because the internalization and recycling of the transferrin receptor is normal in ML4 cells[20], and lysosomal Fe^{2+} release (into the cytosol) is probably mediated directly by an iron-conducting channel/transporter, as is the case for DMT1 (ref. 22). Therefore, by far the simplest explanation of our results is that the Fe^{2+} release pathway between the cytosol and the lysosome lumen is blocked or inactivated in cells with ML4 mutations. Although a ML4-induced loss of Ca^{2+} permeability may result in a defect in lysosomal trafficking and subsequent accumulation of various lipids in LEL, the degradation of these materials is normal[20,21]. Therefore, these accumulated substances would become most harmful only if they are oxidized to generate lipofuscin-like non-degradable materials in the presence of high intralysosomal Fe^{2+} (ref. 19). Lipofuscin-like molecules preferentially accumulate in post-mitotic cells such as muscle cells and neurons, which are primarily affected in ML4 patients[21]. Our work suggests that lysosome-targeting iron chelators might alleviate the degenerative symptoms of ML4 patients.

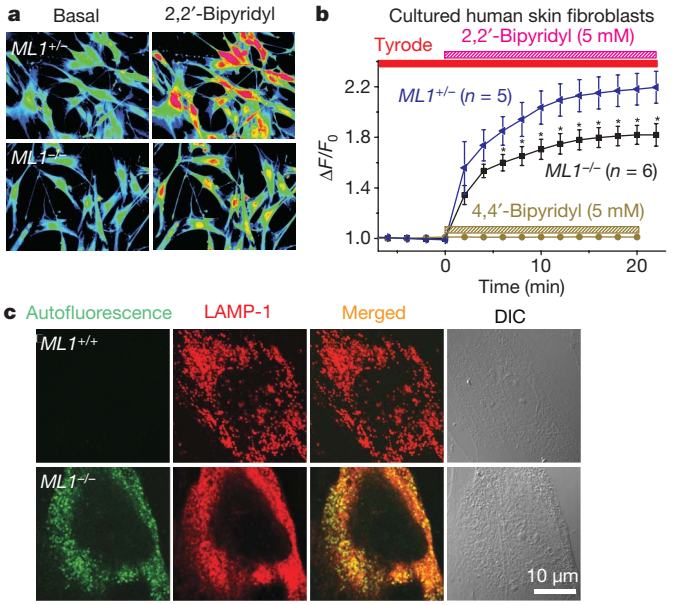

Figure 4 | TRPML1-deficient cells have reduced free (chelatable) iron levels and lysosomal autofluorescence. a, Cultured $TRPML1^{-/-}$ ($ML1^{-/-}$) skin fibroblasts showed less de-quenching of the iron-sensitive fluorescence than $ML1^{+/-}$ cells did. De-quenching was achieved by preloading the fibroblasts with an iron-sensitive dye, Phen Green SK (PG SK), and then adding the membrane-permeable transition metal chelator, 2,2′-bipyridyl (BPD). 2,2′-BPD is predicted to chelate free cellular iron (also referred to as chelatable or labile iron), which subsequently increases PG SK fluorescence. The original magnification used was ×200. **b**, The average 2,2′-BPD induced normalized change of fluorescence ($\Delta F/F_0$) for ML4 cells ($ML1^{-/-}$; $n = 6$ experiments) is significantly (asterisk, $P < 0.01$) lower than for the parental $ML1^{+/-}$ cells. Fibroblast cells ($n = 10$–20) were analysed for each individual experiment. 4,4′-BPD, a 2,2′-BPD analogue that cannot bind Fe^{2+}, did not induce any significant restoration of PG SK fluorescence. Error bars, s.e.m. **c**, An $ML1^{-/-}$ skin fibroblast cell showed autofluorescence in LAMP1-positive compartments. Autofluorescence (green) was detected within a range of excitation wavelengths (shown with excitation at 480 nm). No significant autofluorescence was observed for a $ML1^{+/+}$ cell. Lysosomes were stained with a LAMP1 antibody (red). Differential interference contrast (DIC) images are shown for comparison.

From the cell biology perspective, an important question to address is how TRPML channels are regulated by various cytosolic and luminal factors, and/or by proteins and lipids in the LEL membrane, especially those of which are known to be involved in endolysosomal trafficking.

METHODS SUMMARY

Endolysosomal electrophysiology. HEK293T cells were either transfected with EGFP–TRPML1 alone or co-transfected with mCherry–TRPML1 and EGFP–LAMP1 (a marker for LEL). The size of the LEL is usually $<0.5\,\mu m$, which is suboptimal for patch clamping. We therefore treated cells with 1 μM vacuolin-1 (for 1–2 h), a small chemical known to increase the size of endosomes and lysosomes selectively[23]. Large vacuoles (up to 3 μm; capacitance $= 321 \pm 101$ fF, $n = 11$) were observed in most vacuolin-treated cells (Supplementary Fig. 15). Occasionally, enlarged LEL could also been obtained from TRPML1-transfected cells without vacuolin-1 treatment. No significant difference in TRPML channel properties was seen for enlarged LEL with or without vacuolin-1 treatment. The vacuoles that were positive for both mCherry–TRPML1 and EGFP–LAMP1 were considered as enlarged LEL. Whole-lysosome, lysosome-attached and lysosome luminal-side-out recordings were performed on isolated enlarged LEL, similar to what was performed in enlarged endosomes[24]. In brief, a patch pipette (electrode) was pressed against a cell and then quickly pulled away from the cell to slice the cell membrane. Enlarged LEL were released into the dish and identified by monitoring the TRPML1–EGFP, the TRPML1–mCherry or the LAMP1–EGFP fluorescence.

Iron quenching imaging. HEK293T cells were loaded with 5 μM Fura-2 AM (Molecular Probes) in culture medium at 37 °C for 60 min. Cells were washed in Tyrode's solution for 10–30 min and fluorescence intensity at wavelength 360 nm (F_{360}) was recorded on an EasyRatioPro system (Photon Technology International). EGFP-positive cells were identified by monitoring fluorescence intensity at wavelength 470 nm (F_{470}). Images were analysed using ERP software.

Full Methods and any associated references are available in the online version of the paper at www.nature.com/nature.

Received 26 March; accepted 1 August 2008.
Published online 14 September 2008.

1. Venkatachalam, K., Hofmann, T. & Montell, C. Lysosomal localization of TRPML3 depends on TRPML2 and the mucolipidosis-associated protein TRPML1. *J. Biol. Chem.* **281,** 17517–17527 (2006).
2. Clapham, D. E. TRP channels as cellular sensors. *Nature* **426,** 517–524 (2003).
3. Nilius, B., Owsianik, G., Voets, T. & Peters, J. A. Transient receptor potential cation channels in disease. *Physiol. Rev.* **87,** 165–217 (2007).
4. Bassi, M. T. *et al.* Cloning of the gene encoding a novel integral membrane protein, mucolipidin-and identification of the two major founder mutations causing mucolipidosis type IV. *Am. J. Hum. Genet.* **67,** 1110–1120 (2000).
5. Sun, M. *et al.* Mucolipidosis type IV is caused by mutations in a gene encoding a novel transient receptor potential channel. *Hum. Mol. Genet.* **9,** 2471–2478 (2000).
6. Hentze, M. W., Muckenthaler, M. U. & Andrews, N. C. Balancing acts: molecular control of mammalian iron metabolism. *Cell* **117,** 285–297 (2004).
7. Lee, D. W., Andersen, J. K. & Kaur, D. Iron dysregulation and neurodegeneration: the molecular connection. *Mol. Interv.* **6,** 89–97 (2006).
8. Kidane, T. Z., Sauble, E. & Linder, M. C. Release of iron from ferritin requires lysosomal activity. *Am. J. Physiol. Cell Physiol.* **291,** C445–C455 (2006).
9. Gunshin, H. *et al.* Slc11a2 is required for intestinal iron absorption and erythropoiesis but dispensable in placenta and liver. *J. Clin. Invest.* **115,** 1258–1266 (2005).
10. Pryor, P. R., Reimann, F., Gribble, F. M. & Luzio, J. P. Mucolipin-1 is a lysosomal membrane protein required for intracellular lactosylceramide traffic. *Traffic* **7,** 1388–1398 (2006).
11. Xu, H., Delling, M., Li, L., Dong, X. & Clapham, D. E. Activating mutation in a mucolipin transient receptor potential channel leads to melanocyte loss in varitint-waddler mice. *Proc. Natl Acad. Sci. USA* **104,** 18321–18326 (2007).
12. Di Palma, F. *et al.* Mutations in *Mcoln3* associated with deafness and pigmentation defects in varitint-waddler (*Va*) mice. *Proc. Natl Acad. Sci. USA* **99,** 14994–14999 (2002).
13. Altarescu, G. *et al.* The neurogenetics of mucolipidosis type IV. *Neurology* **59,** 306–313 (2002).
14. Goldin, E. *et al.* Transfer of a mitochondrial DNA fragment to *MCOLN1* causes an inherited case of mucolipidosis IV. *Hum. Mutat.* **24,** 460–465 (2004).
15. Bargal, R., Goebel, H. H., Latta, E. & Bach, G. Mucolipidosis IV: novel mutation and diverse ultrastructural spectrum in the skin. *Neuropediatrics* **33,** 199–202 (2002).
16. Kress, G. J., Dineley, K. E. & Reynolds, I. J. The relationship between intracellular free iron and cell injury in cultured neurons, astrocytes, and oligodendrocytes. *J. Neurosci.* **22,** 5848–5855 (2002).
17. Petrat, F., de Groot, H. & Rauen, U. Determination of the chelatable iron pool of single intact cells by laser scanning microscopy. *Arch. Biochem. Biophys.* **376,** 74–81 (2000).
18. Goldin, E., Blanchette-Mackie, E. J., Dwyer, N. K., Pentchev, P. G. & Brady, R. O. Cultured skin fibroblasts derived from patients with mucolipidosis 4 are autofluorescent. *Pediatr. Res.* **37,** 687–692 (1995).
19. Kurz, T., Terman, A., Gustafsson, B. & Brunk, U. T. Lysosomes in iron metabolism, ageing and apoptosis. *Histochem. Cell Biol.* **129,** 389–406 (2008).
20. Chen, C. S., Bach, G. & Pagano, R. E. Abnormal transport along the lysosomal pathway in mucolipidosis, type IV disease. *Proc. Natl Acad. Sci. USA* **95,** 6373–6378 (1998).
21. Zeevi, D. A., Frumkin, A. & Bach, G. TRPML and lysosomal function. *Biochim. Biophys. Acta.* **1772,** 851–858 (2007).
22. Andrews, N. C. & Schmidt, P. J. Iron homeostasis. *Annu. Rev. Physiol.* **69,** 69–85 (2007).
23. Cerny, J. *et al.* The small chemical vacuolin-1 inhibits Ca^{2+}-dependent lysosomal exocytosis but not cell resealing. *EMBO Rep.* **5,** 883–888 (2004).
24. Saito, M., Hanson, P. I. & Schlesinger, P. Luminal chloride-dependent activation of endosome calcium channels: patch clamp study of enlarged endosomes. *J. Biol. Chem.* **282,** 27327–27333 (2007).

Supplementary Information is linked to the online version of the paper at www.nature.com/nature.

Acknowledgements This work is supported by start-up funds to H.X. from the Department of Molecular, Cellular, and Developmental Biology and Biological Science Scholar Program, University of Michigan. We thank U. Brunk, M. Saito, R. Hume, C. Duan, M. Akaaboune, J. Kuwada, S. Low, S. Punthambaker and S. Dellal for assistance, and D. Clapham, N. Andrews, L. DeFelice, L. Yue, D. Ren, C. Jiang and S. Xu for comments on an earlier version of the manuscript. We also thank K. Kiselyov for sharing his unpublished results on lysosomal iron staining of ML4 cells. We appreciate the encouragement and helpful comments from other members of the Xu laboratory.

Author Information Reprints and permissions information is available at www.nature.com/reprints. Correspondence and requests for materials should be addressed to H.X. (haoxingx@umich.edu).

METHODS

Molecular biology and biochemistry. Full-length mouse TRPML1 and TRPML3, and a short splicing variant of mouse TRPML2 (GeneBank accession NP_001005846), were cloned into the EGFP-C2 vector (Clontech), the mCherry vector, or haemagglutinin-tag containing pcDNA3 as described previously[11]. No significant functional difference was observed among EGFP-tagged, mCherry-tagged and haemagglutinin-tagged $TRPML^{Va}$ constructs. ML4 mutants were constructed on a $TRPML1^{Va}$ background using a site-directed mutagenesis kit (Qiagen). All constructs were confirmed by sequencing analysis and protein expression was verified by western blotting. HEK293T cells were transiently transfected with wild-type TRPML1, $TRPML1^{Va}$ and ML4 mutants for electrophysiology, confocal imaging, $^{55}Fe^{2+}$ uptake and Fe^{2+} quenching assays. TRPML1 western blot analyses were performed with an anti-EGFP monoclonal antibody (Covance).

Confocal imaging. All images were taken using a Leica (TCS SP5) confocal microscope. LAMP1 antibody was from the Iowa Hybridoma Bank and LysoTracker was from Molecular Probes (Invitrogen).

Mammalian cell electrophysiology. Recordings were performed in transiently transfected HEK293T cells. Cells were cultured at 37 °C, transfected using Lipofectamine 2000 (Invitrogen) and plated onto glass coverslips. No significant difference was observed for EGFP-tagged versus untagged $TRPML1^{Va}$-transfected cells. Unless otherwise stated, pipette solution contained 147 mM Cs, 120 mM methanesulphonate (MSA), 4 mM NaCl, 10 mM EGTA, 2 mM Na_2-ATP, 2 mM $MgCl_2$, 20 mM HEPES (pH 7.2; free $[Ca^{2+}]_i < 10$ nM). Standard extracellular bath solution (modified Tyrode's solution) contained 153 mM NaCl, 5 mM KCl, 2 mM $CaCl_2$, 1 mM $MgCl_2$, 20 mM HEPES and 10 mM glucose (pH 7.4). To reduce the background from an endogenous Cl^- conductance activated by protons that was strongly outwardly rectifying[11,25], gluconate$^-$ or MSA^- was used to replace most of the Cl^- (remaining $[Cl^-]_o = 5$–10 mM) for all low-pH bath solutions. Low-pH 'Tyrode's' solution contained 150 mM Na-gluconate, 5 mM KCl, 2 mM $CaCl_2$, 1 mM $MgCl_2$, 10 mM glucose, 10 mM HEPES and 10 mM MES (pH 4.6). $NMDG^+$ solution contained 160 mM NMDG, 20 mM HEPES, 10 mM glucose (pH 7.4). Low-pH $NMDG^+$ solution contained 150 mM NMDG, 10 mM glucose, 10 mM MES, 10 HEPES (pH adjusted to 4.6 using MSA). 'Isotonic' metal solutions contained 105 mM metal ions, 30 mM glucose, 10 mM HEPES, 10 mM MSA and 0–30 mM $NMDG^+$ (pH 4.6). Further metal solutions (1, 3, 10 and 30 mM) were derived from mixing isotonic solutions with low-pH $NMDG^+$ solutions at various ratios. Monovalent (nominal divalent-free) solutions contained 10 mM glucose, 20 mM HEPES, 160 mM NaCl and 5 mM KCl (pH 7.4; free Ca^{2+} <1–10 μM). All solutions were applied by a fast perfusion system to achieve a complete solution exchange within a few seconds. Data were collected using an Axopatch 2A patch clamp amplifier, Digidata 1440 and pClamp 10.0 software (Axon Instruments). Whole-cell currents and single channel recordings were digitized at 10 kHz and filtered at 2 kHz. Capacity current was reduced as much as possible using the amplifier circuitry. Series resistance compensation was 60%–85%. All experiments were conducted at room temperature (~21–23 °C) and all recordings were analysed with pCLAMP10 (Axon Instruments) and Origin 7.5 (Origin Lab).

Iron de-quenching imaging. Cultured skin fibroblast cells from a ML4 patient ($TRPML1^{-/-}$, clone WG0909) and corresponding heterozygous parent ($TRPML1^{+/-}$, clone WG0987) were obtained from the Repository for Mutant Human Cell Strains of Montreal Children's Hospital (Montreal, Canada). Fibroblast cells were loaded with 20 μM Phen Green SK (Molecular Probes) in culture medium at 37 °C for 20 min followed by a 15 min wash. Cellular fluorescence was excited at 488 nm on the PTI ERP system. Quenching of fluorescence was induced by the addition of the membrane-permeable transition metal chelator 2,2′-bipyridyl (5 mM)[17]. The 2,2′-bipyridyl analogue 4,4′-bipyridyl, which cannot bind or chelate Fe^{2+}, was used as a control. Because many variables such as dye loading may contribute to the variation of basal fluorescence (F) of PG SK, the normalized change of fluorescence ($\Delta F/F$) was used as readout to estimate the change in cytosolic Fe^{2+} levels.

Iron uptake assay. Iron uptake was measured as described previously[25]. In brief, 30 h after transfection, HEK293T cells were washed twice with prewarmed PBS and then incubated with 1 ml of prewarmed uptake assay buffer (25 mM Tris, 25 mM MES, 140 mM NaCl, 5.4 mM KCl, 5 mM glucose, 1.8 mM $CaCl_2$, 800 μM MgSO4, 50 μM ascorbic acid, pH 5.8) containing ^{55}Fe-nitrilotriacetic acid (NTA, 1 μM ^{55}Fe) at 37 °C for 5 min. ^{55}Fe-NTA was made by mixing $^{55}FeCl_3$ (PerkinElmer) with 100 mM NTA in a 1:50 molar ratio. Ascorbic acid (100 mM) was used to promote the formation and maintenance of ferrous (Fe^{2+}) iron (adjusted to pH 5.8). All uptake assays were performed with 20 μM Fe^{2+} (with a 1:20 molar ratio for $^{55}FeCl_3$ and $FeSO_4$) at pH 5.8. Assays were stopped by the addition of 2 ml ice-cold PBS. After washing three times with ice-cold PBS, the cells were detached and collected by adding 1 ml 0.25% trypsin-EDTA. Parallel experiments were conducted at 0 °C to measure the cell surface ^{55}Fe binding, which was subtracted from the values at 37 °C to obtain the net iron uptake. Cell-associated radioactivity was measured with liquid scintillation spectrometry.

Lysosomal iron staining. Lysosome iron was stained using a modified sulphide-silver method[19]. In brief, fibroblast cells were grown on coverslips and exposed to 50 μM Fe^{3+}-dextran overnight. Cells were then washed with PBS and fixed with 2% glutaraldehyde in 0.1 M Na-cacodylate buffer with 0.1 M sucrose (pH 7.2) for 1.5 h at room temperature (22 °C). Next cells were sulphidated at ~pH 9 with 1% (w/v) ammonium sulphide in 70% (v/v) ethanol for 15 min. The development was then performed using a physical, colloid-protected developer containing silver-lactate and hydroquinone for 1–2 h.

Reagents. 2,2'-BPD, 4,4'-BPD, iron ascorbate, ferric chloride, iron dextran, and all other metal salts were from Sigma Chemicals.

Data analysis. Most data are presented as the mean ± s.e.m. Statistical comparisons were made using analysis of variance (ANOVA). A P value < 0.05 was considered statistically significant.

25. Xu, H., Jin, J., DeFelice, L. J., Andrews, N. C. & Clapham, D. E. A spontaneous, recurrent mutation in divalent metal transporter-1 exposes a calcium entry pathway. *PLoS Biol.* **2**, E50 (2004).